Journal of Ceramic Processing Research. Vol. 5, No. 1, pp. 18~24 (2004)

J O U R N A L O F
Ceramic Processing Research

Properties and performance of spark plasma sintered, laminated WC-Co cutting tools

K.M. Fox*, J.R. Hellmann, H. Izui[a], M.F. Amateau[b], W. Fu[c] and P.H. Cohen[c]

Department of Materials Science and Engineering, The Pennsylvania State University
[a]Department of Aerospace Engineering, College of Science and Technology, Nihon University, Chiba 274-8501, Japan
[b]Department of Engineering Science and Mechanics, The Pennsylvania State University
[c]Department of Industrial and Manufacturing Engineering, The Pennsylvania State University, University Park, PA 16802, U.S.A.

The goal of the study was to fabricate laminated WC-Co cutting tools with residual thermoelastic stress states tailored to counteract the thermal and mechanical stresses imposed by machining. Cutting tools were fabricated using tape casting and bulk powder compaction of submicrometre and nanograin WC-Co powders. The weight fraction of cobalt in the tool was graded to produce residual compressive stresses in the tool surface. Spark plasma sintering (SPS) was used to fully densify the laminates while suppressing cobalt redistribution via sub-eutectic (solid state) sintering. Microstructural analysis showed that the cobalt binder was not well distributed around the WC grains after sintering. Contiguity of the WC grains was high, and segregation of cobalt was apparent. These factors are expected to hinder machining performance. However, the laminated tools performed similarly to commercially-available, monolithic tools in turning Ti-6Al-4V alloy. This demonstrates that the incorporation of residual stresses into the surface of the tool is beneficial for wear resistance. Refinement of powder processing methods to produce laminated WC-Co tools with a better distribution of cobalt should yield a further increase in machining performance.

Key words: Spark plasma sintering, tungsten carbide cobalt, laminated composites.

Introduction

Cemented carbides, particularly WC-Co, have been extensively employed as cutting tools because they possess a combination of both high hardness and high fracture toughness. Tungsten carbide grains are very hard and wear resistant, and the addition of cobalt metal provides a ductile matrix for increased fracture toughness. Most plastic deformation occurs in the cobalt binder phase, although the WC phase acts to increase the yield strength of the binder through mechanical restraint [1]. This is closely related to the binder mean free path [2]. Typically, as the binder mean free path approaches zero (smaller weight fractions of cobalt), fracture toughness is reduced. WC grain size also has a strong affect on fracture toughness and strength of the composite. A reduction in WC grain size yields increased hardness and strength, but reduced fracture toughness [3].

Recent studies have shown that when WC grain size is reduced to the nanometre range, fracture toughness remains constant while hardness increases [4]. This improvement in fracture toughness was attributed to the uniformity of the microstructure, including carbide grain size and cobalt distribution. Recently, more specific differences in toughening mechanisms between conventional and nanograin WC-Co composites have been examined [5, 6]. Toughening in conventional WC-Co composites is based on crack tip shielding due to plastic deformation in the cobalt binder phase, while crack bridging has been observed in WC-Co nanocomposites [6]. Nanograin WC-Co composites exhibit increased wear resistance because the binder matrix is exposed to the abrasive environment over smaller dimensions, and macroscopic hardness is typically higher than that of conventional grain size materials [5]. Therefore, retention of nanocrystallinity is of interest for enhanced tool performance. However, conventional liquid phase sintering methods for production of WC-Co composites result in microstructural coarsening, eliminating the benefits of nanocrystallinity. For this reason, alternative processing and sintering techniques must be developed to exploit the benefits of nanograin WC-Co composites for cutting tool applications.

Spark plasma sintering (SPS) should be beneficial in sintering laminated WC-Co structures because shorter sintering times at sub-eutectic (solid-state) sintering temperatures will prevent homogenization of the graded cobalt structure. The short, low temperature sintering cycles made possible by SPS should minimize grain

*Corresponding author:
Tel : +814-865-0163
Fax: +814-865-0016
E-mail: jrh3@ems.psu.edu

growth. In addition, SPS might eliminate the need for grain growth inhibitors, which have been shown to adversely affect the performance of cemented carbides [7].

Spark plasma sintering is a relatively new technology for rapid densification of materials. SPS involves consolidation of a powder compact by direct application of a pulsed DC current and uniaxial pressure in a graphite die [8]. Several factors have been reported to contribute to densification by SPS: spark plasma generation between powder particles, spark impact pressure, Joule heating, an electrical field-enhanced diffusion effect, and plastic deformation due to applied pressure [9]. The plasma momentarily generated at gaps between particles results in localized heating to very high temperatures. The powder surfaces melt and evaporate, forming necks between particles and result in condensation of the evaporated species in the non-neck regions. Surface impurities and gases adsorbed onto the particle surfaces are removed by the plasma, resulting in cleaner surfaces which sinter much faster than in regular sintering processes [10]. Diffusion rates have also been reported to increase by the application of the field because of the electric field-enhanced migration of ions [9].

The purpose of this study is to investigate the utility of SPS to suppress grain growth and structural homogenization of laminated WC-Co tools, and to study the machining performance of these tools relative to conventional, monolithic tools.

Experimental Procedure

Laminated structural designs composed of a low cobalt weight fraction case and a higher cobalt weight fraction core were selected for the cutting tool inserts (Fig. 1). Laminates of five different designs were fabricated, as listed in Table 1. Designs were chosen to maximize the difference in cobalt content between the case and core, within the limits of the available powders.

Submicrometre WC, Co and VC powders, and nanograin WC-Co powders were examined in an effort to assess the effect of sintering methods on retaining fine grain size. The submicrometre WC powder was jet milled to a particle size of 0.7-0.9 μm by the manufacturer [11]. The nanograin WC-Co powder was produced by the spray conversion technique [12, 13], and has a reported mean crystallite size of 20-40 nm [14]. Nevertheless, a large amount of agglomeration was apparent in the nanograin powder. Particle size measurements were made using the line intercept method on scanning electron micrographs at magnifications where primary particles could be resolved (Fig. 2 and Fig. 3). The results are shown in Table 2. The agglomerated nanograin powders appear similar in size to the submicrometre powders, but are comprised of smaller crystallites.

Tape casting was used to fabricate the outer layer (case) of the laminated tools since careful control of the case thickness is necessary to tailor residual stresses. The carbide powders were dispersed in a slip containing an organic binder and solvent, as shown in Table 3. Vanadium carbide was added at 0.6 wt.% as a grain growth inhibitor to some compositions.

Spark plasma sintering (SPS) was utilized to densify the laminated tools. A Dr. Sinter 3.20 MK-IV, manufactured by Sumitomo Coal Mining, Ltd., was used. A 30 mm diameter graphite die set, coated with BN, was loaded sequentially with tape and WC-Co powder. The powder and tape were pre-compacted at 20 MPa before

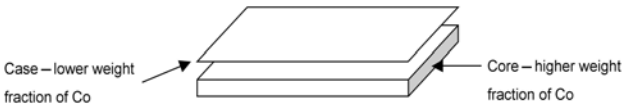

Fig. 1. Schematic of the basic laminated tool design.

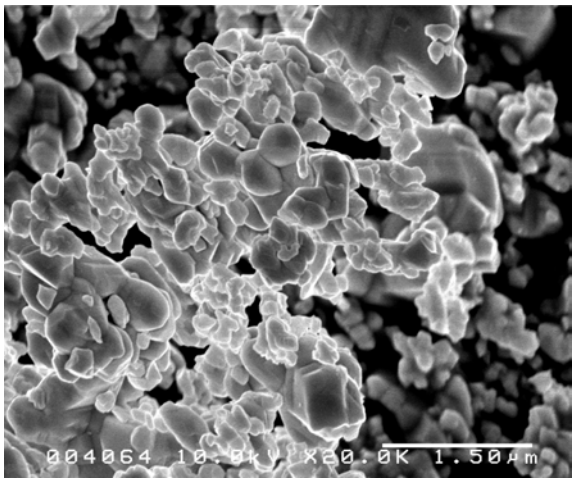

Fig. 2. FE-SEM micrograph of submicrometre WC-Co powder (4 wt.% Co).

Table 1. Composition of laminated tools produced by SPS

Laminate design designation	Weight percent Co in case	Weight percent Co in core	Sintering temperature (°C)
Nanograin 5-8	5	8	1125
Nanograin 5-8 with VC added	5	8	1150
Submicrometre 4-10	4	10	1125
Submicrometre 6-10	6	10	1125
Nanograin case / Submicrometre Core 5-10	5	10	1125

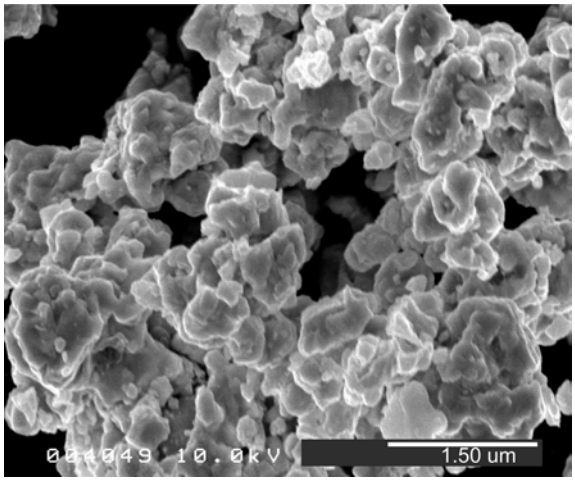

Fig. 3. SEM micrograph of nanograin WC-Co powder (5 wt.% Co).

Table 2. Particle size of WC-Co powders measured by line intercept

Powder type	Mean particle size (μm)
Submicrometre 4 wt.% Co with VC	0.370
Submicrometre 10 wt.% Co with VC	0.373
Nanograin 5 wt.% Co	0.480
Nanograin 5 wt.% Co with VC	0.447
Nanograin 8 wt.% Co	0.309
Nanograin 8 wt.% Co with VC	0.210

Table 3. Slip formulation for tape casting of WC/Co/VC powders

Material	Role	Weight percent
Ethyl methacrylate	Binder	6.4
Methyl ethyl ketone	Solvent	5.7
95% ethyl alcohol	Solvent	4.7
Dibutyl phthalate	Plasticizer	0.6
Mixed WC/Co/VC powder		82.6

being placed in the SPS chamber. A vacuum atmosphere of less than 10^{-3} atm was used. The heating rate was 100 K min^{-1}, and applied pressure was 50 MPa. Sintering time was 10 minutes, and sintering temperature was varied depending on the cobalt content of the case, as listed in Table 1.

The density of each specimen was measured by Archimedes method using calibrated kerosene as the immersion liquid, following ASTM B311 and D891. Reflected light microscopy was utilized to examine polished specimens for open porosity and uncombined carbon, following ASTM B276 and B657. Murakami's etchant, described in ASTM E407, was used to reveal the WC-Co interfaces. Scanning electron microscopy (SEM) was used to image polished and etched cross-sections of the tools. Electron probe microanalysis (EPMA) was used to image the laminated structure.

The mean intercept diameter of the WC grains, contiguity of WC grains, and mean free path of the cobalt binder were determined using the line intercept methods described by ASTM E112 and Underwood [15]. The hardness of the case layer and core layer of each specimen was measured with a Vickers indenter following ASTM C1327.

Fracture toughness was estimated by measuring the lengths of the cracks introduced during Vickers indentation using the relationships developed by Ponton and Rawlings for use with WC-Co composites [16, 17]:

$$K_c = \frac{0.0319P}{al^{0.5}} \quad (1)$$

P is the load applied, a is the half-width of the indent diagonal and l is the length of the crack extending from the corner of the indent along the surface of the material. This equation assumes that the cracks formed by the Vickers indenter are Palmqvist cracks, which has been shown to be the correct crack morphology in WC-Co [17, 18]. The Palmqvist crack length in WC-Co has only a small dependence on the indenter load (a change of about 1.5% per 100 N increase) [19], so only one load was used in this study. The indentation method of fracture toughness measure-ment is very sensitive to surface stresses, since they can enhance or reduce crack lengths considerably [19]. Specimens evaluated in this study were carefully polished with diamond suspensions to an optical finish, as this has been shown to remove residual stresses left from cutting and grinding [20]. Crack lengths were measured immediately after indentation to minimize the effect of any slow crack growth.

Residual strain in the surface of the sintered tools was measured by XRD. A Philips X'PERT MRD was used, with Cu Kα radiation. Residual stresses were calculated by the $\sin^2\Psi$ technique using the WC (211) peak. Values of 720 GPa and 0.18 were used for Young's modulus and Poisson's ratio of WC, respectively [21]. The standard deviation in the stress measurements accounts for goniometer precision, quality of the Pearson VII peak fit, and quality of the linear fit to the $\sin^2\Psi$ data.

The performance of the laminated cutting tools was evaluated using an instrumented turning operation. Titanium-6Al–4V was chosen as the alloy for use in the performance tests because its low thermal conductivity makes it difficult to machine with standard tools. The tools were tested under harsh cutting conditions (relative to conventional industrial practice) in order to maximize wear rates and to minimize the amount of Ti-6Al-4V that was consumed due to its high cost. Cutting speed was 200 fpm (1.52 m/s), feed rate was 0.0052 in./rev. (135 mm/rev.), and depth of cut was 0.070 in. (1.78 mm). The inserts were flooded with a coolant/lubricant during the cuts. Flank wear was quantified using a video measuring system attached to an optical microscope. Kennametal's commercially available K313 cutting

tool insert (6 wt.% Co) was used as a standard by which to compare the performance of the laminated tools.

Results and Discussion

All specimens were greater than 99.8% dense (Table 4). No porosity or uncombined carbon was observed under reflected light microscopy. Elemental mapping with electron probe microanalysis (EPMA) confirmed that the laminated structure was retained after sintering, as shown in Fig. 4. The measured values of WC grain size are listed in Table 4. These values should be regarded as estimates; the actual grain sizes are distributed over a range of dimensions. There was not enough contrast between the WC and Co in SEM micrographs to enable use of quantitative microscopy for grain size distribution measurements.

Vickers microhardness data for the monolithic and laminated tools appear in Table 5. The fracture toughness values measured by indentation are shown in Table 6. Residual stresses in the case layers of the laminated tools complicate the measurement of fracture toughness by indentation and surface crack measurement. Only the cracks that ran parallel to the direction of the expected residual stresses in the case layers of the laminated tools were measured in order to minimize the effect of the residual compression on crack length.

Table 4. Properties of laminated tools and Kennametal's K313

Laminate design designation	Density (% theoretical)	Mean grain size, μm (std. dev.)
Nanograin 5-8	99.8%	0.510 (0.114)
Nanograin 5-8 with VC added	99.9%	0.422 (0.091)
Submicrometre 4-10	100%	0.478 (0.109)
Submicrometre 6-10	100%	0.415 (0.077)
Nanograin case / Submicrometre core 5-10	100%	0.437 (0.116)
K313	100%	0.733 (0.200)

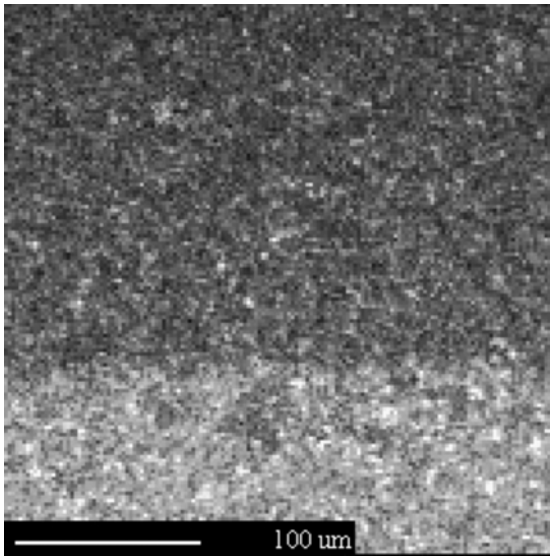

Fig. 4. EPMA elemental map showing the distribution of cobalt near the surface of a submicrometre 4-10 laminated tool. The top layer is 4 wt.% Co, and the bottom layer is 10 wt.% Co.

Table 5. Vickers microhardness of laminated tools and K313

Laminate design designation	Mean Vickers hardness number, case (GPa)	Standard deviation (GPa)	Number of measurements	Mean Vickers hardness number, core (GPa)	Standard deviation (GPa)	Number of measurements
Nanograin 5-8	2095 (20.5)	77.6 (0.8)	10	1760 (17.3)	43.4 (0.4)	10
Nanograin 5-8 with VC added	2359 (23.1)	165.9 (1.6)	10	1871 (18.3)	21.0 (0.2)	10
Nanograin case / Submicrometre core 5-10	2043 (20.0)	24.9 (0.2)	10	1795 (17.6)	35.5 (0.3)	10
Submicrometre 4-10	2312 (22.7)	40.0 (0.4)	10	1821 (17.9)	48.0 (0.5)	10
Submicrometre 6-10	1960 (19.2)	46.3 (0.5)	10	1868 (18.3)	91.8 (0.9)	10
K313				1890 (18.5)	40 (0.4)	25

Table 6. Indentation fracture toughness of laminated tools and K313

Laminate design designation	Mean fracture toughness, case MPa $m^{1/2}$	Standard deviation MPa $m^{1/2}$	Number of measurements	Mean fracture toughness, core MPa $m^{1/2}$	Standard deviation MPa $m^{1/2}$	Number of measurements
Nanograin 5-8	7.84	0.33	5	9.66	1.02	10
Nanograin 5-8 with VC added	9.13	0.62	5	9.52	0.71	10
Nanograin case / Submicrometre core 5-10	7.80	0.22	5	9.44	0.44	10
Submicrometre 4-10	7.44	1.15	5	9.06	0.45	10
Submicrometre 6-10	6.06	0.96	5	10.08	0.19	10
K313				12.82	1.54	10

Indentations in the case layers remained symmetrical.

In general, compositions with higher cobalt content show an expected decrease in microhardness since the cobalt matrix is more susceptible to plastic deformation than WC grains. There was no significant difference in microhardness between the nanograin and the submicrometre specimens. This is likely because of the similar sintered grain sizes and cobalt distribution of both types of specimens.

The mean grain size of the nanograin specimens is larger than that of the submicrometre grain specimens. This is likely due to the extensive agglomeration of the nanograin powders. The nanograin particles may also have been more highly strained, resulting in a larger driving force for recrystallization and grain growth. The nanograin 5-8 design shows a reduction in grain size when VC is added. The submicrometre grain size specimens, represented by Fig. 5, show somewhat rounded grains, and a wide distribution of grain sizes. The nanograin specimens, represented by Fig. 6, show more angular grains. Grain sizes appear to be distributed over a narrower range than the submicrometre grain specimens.

All of the specimens were sintered well below the WC-Co eutectic temperature of 1320°C, and for times of 10 minutes or less. This should have restricted grain growth and migration of cobalt, so that grains are more rounded and the cobalt is not evenly distributed. However, the angularity of the nanograin specimens suggests that significant recrystallization and growth occurred during sintering. A higher degree of strain and greater specific surface area in the nanograin powders may have provided the driving force for this grain growth.

The WC contiguity and cobalt mean free path data are shown in Table 7. The contiguity of WC grains and the mean free path of the cobalt binder are indicators of the distribution of cobalt in the composite structure. A high degree of WC contiguity indicates that many of the grains are in direct contact with each other, and can also be a measure of microstructural homogeneity. The cobalt mean free path is an indicator of the average thickness of the cobalt binder layer between the WC grains. The WC contiguity is relatively high for the SPS specimens because there is a larger amount of cobalt segregation at WC triple points. Fig. 7 shows a representative microstructure for nanograin laminates, and Fig. 8 shows a representative microstructure for submicrometre laminates. This uneven distribution of cobalt in the SPS specimens is a result of sub-eutectic sintering, which limited the ability of the WC grains to rearrange by capillarity. Similarly, cobalt was not able to redistribute evenly between the WC grains. The inhomogeneity of WC and Co in the starting powders was not homogenized during solid state sintering.

The inconsistency of fracture toughness values are likely due to the uneven distribution of cobalt and high contiguity of WC grains. The lack of the cobalt binder

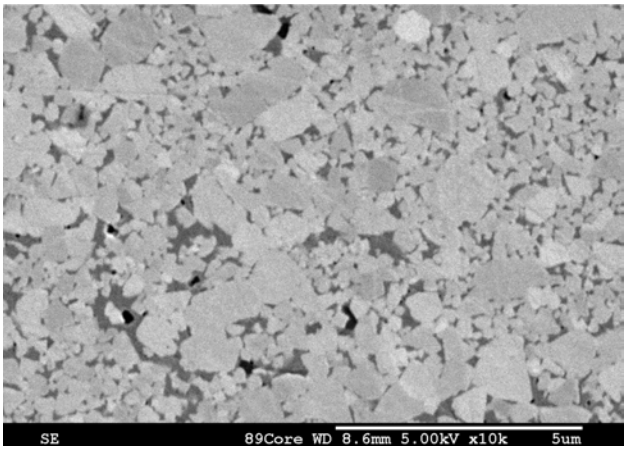

Fig. 5. SEM micrograph of the core region of a submicrometre 6-10 laminate sintered by SPS. Grains are more rounded, and grain size distribution appears to be wide.

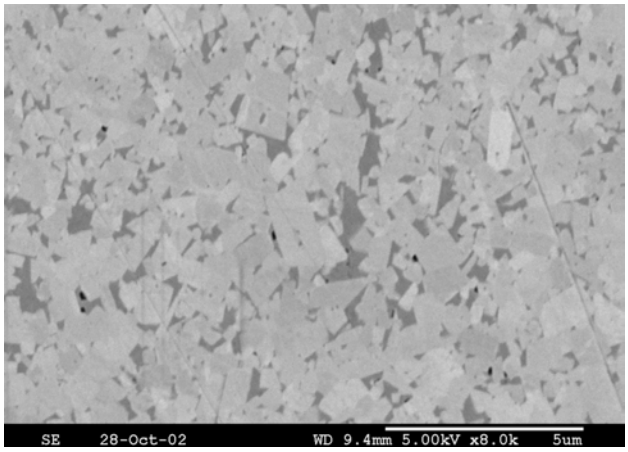

Fig. 6. SEM micrograph of the case region of a nanograin 5-8 laminate specimen. Grains are angular, and appear to be distributed over a narrower range of sizes than the submicrometre grain specimens.

Table 7. WC contiguity and cobalt mean free path of laminated tools and K313

Laminate design designation	WC contiguity	Standard deviation	Co mean free path (μm)	Standard deviation (μm)
Nanograin 5-8	0.67	0.13	0.19	0.09
Nanograin 5-8 with VC added	0.57	0.10	0.12	0.03
Submicrometre 4-10	0.47	0.17	0.15	0.06
Submicrometre 6-10	0.56	0.13	0.16	0.07
Nanograin case / Submicrometre core 5-10	0.55	0.18	0.19	0.15
K313	0.56	0.21	0.18	0.11

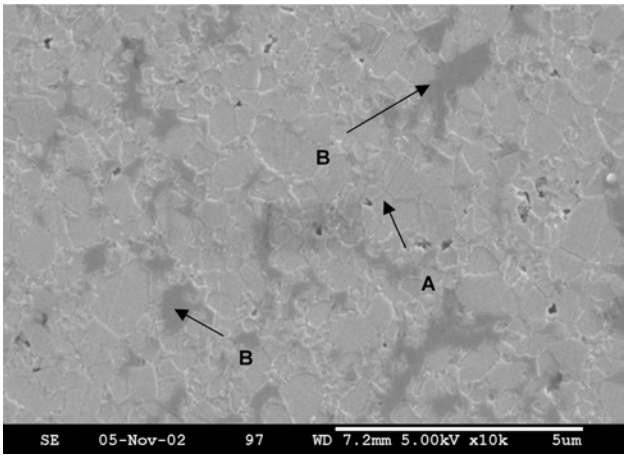

Fig. 7. SEM micrograph of a nanograin 5-8 laminate specimen. The arrow marked A shows WC grain boundaries with no cobalt binder. The arrows marked B show pools of the cobalt binder.

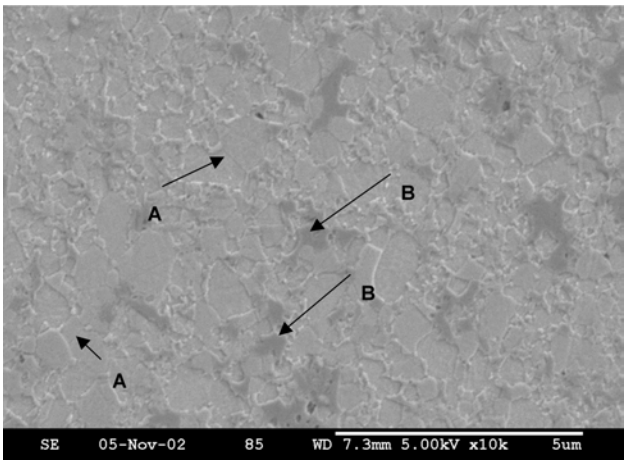

Fig. 8. SEM micrograph of a submicrometre 4-10 laminate. The arrows marked A show WC grain boundaries with no cobalt binder. The arrows marked B show pools of the cobalt binder.

phase between each grain reduces the amount of crack tip shielding that can occur in the composite. A previous study has verified that increased carbide contiguity reduces fracture toughness [22].

Residual compressive stress in the surface of the laminated tools was confirmed by X-Ray diffraction. Table 9 shows the residual stresses in both monolithic and laminated tools sintered by SPS. The laminated tools clearly show a higher degree of compressive stress in the low cobalt-containing case compared to the monolithic tools. The 10 wt.% cobalt tools may have lower residual stress values due to a greater amount of plastic deformation in the cobalt matrix during cooling, which relieves some of the strain. Surface preparation for machining will further modify the residual stress state in the surface of the laminated tools. A study of these effects is underway.

Instrumented machining tests were performed after the tools were ground and honed. Cutting was stopped at 3-minute intervals and the length of the flank wear

Table 9. Residual surface stresses

Laminate design designation	Residual Stress (MPa)	Standard Deviation (MPa)
Monolithic 8% Co	-394	154
Nanograin 5-8	-1707	203
Monolithic 10% Co	-146	44
Submicrometre 4-10	-1132	128

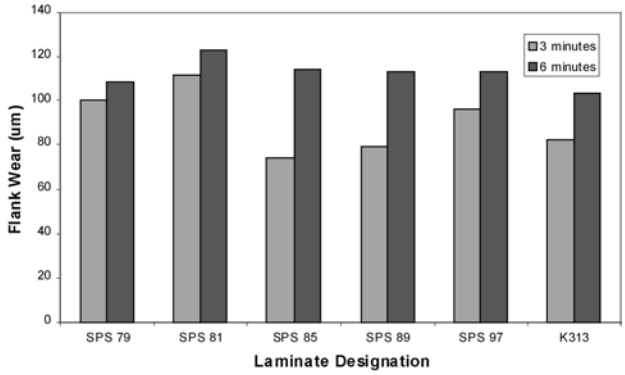

Designation	Laminate Design
SPS 79	Submicron 10% Monolithic
SPS 81	Nano 5-8 Laminate
SPS 85	Submicron 4-10 Laminate
SPS 89	Submicron 6-10 Laminate
SPS 97	Nanograin 8% Monolithic
K313	Submicron 6% Monolithic

Fig. 9. Instrumented cutting data for tools sintered by SPS. Kennametal's K313 tool is used for comparison.

scar was measured. Two edges of each laminated tool and three edges of K313 tools were evaluated. The data for 3 and 6 minutes of cutting appear in Fig. 9. After 6 minutes of cutting, there was little difference in average flank wear between the laminated tools and Kennametal's K313 cutting tool insert. There was also little difference in flank wear between the laminated and monolithic tools sintered by SPS.

Conclusions

Laminated WC-Co cutting tools were fabricated using tape casting and bulk powder compaction of submicrometre and nanograin powders. Spark plasma sintering (SPS) was successful in producing fully dense tools and in maintaining the graded cobalt structure by sintering for short times at temperatures below the WC-Co eutectic. SPS also minimized grain growth when submicrometre WC-Co powders were used. EPMA confirmed that homogenization of the graded cobalt structure did not occur, and XRD indicated a high degree of residual compressive stress in the surface of the laminated tools.

The case layers of the laminated tools have higher hardness and lower fracture toughness values than the core, as expected. Microstructural analysis of the SPS tools showed that the cobalt binder was not well distributed around the WC grains. Contiguity of the

WC grains was high, and segregation of cobalt was apparent.

An uneven distribution of cobalt is expected to be detrimental to machining performance of WC-Co tools. However, the laminated tools produced in this study showed cutting performance that was similar to that of commercially available, monolithic tools. This demonstrates that the incorporation of residual stresses into the surface of the tool is beneficial for wear resistance.

Refinement of powder processing methods to produce laminated WC-Co composites with a more homogenous distribution of cobalt should yield a further increase in machining performance. Sub-eutectic densification by SPS could be a useful method of maintaining a compositional gradient and a small grain size while achieving full density in materials that are typically liquid phase sintered.

Acknowledgements

This research is supported by the Center for Innovative Sintered Products at The Pennsylvania State University. Spark plasma sintering work was funded by the National Science Foundation Summer Programs in East Asia. The authors gratefully appreciate the support of Sumitomo Coal Mining Co., Ltd., and Nihon University, Japan.

References

1. E.M. Trent, and P.K. Wright, “Metal Cutting” (Butterworth-Heinemann, 2000).
2. J. Gurland, and P. Bardzil, Transactions of the Metallurgical Society of AIME 203 (1955) 311-315.
3. J. Gurland, Transactions of the Metallurgical Society of AIME 227 (1963) 1146-1150.
4. R. Porat, S. Berger, and A. Rosen, Materials Science Forum 225-227 (1996) 629-634.
5. K. Jia, and T.E. Fischer, Materials Research Society Symposium Proceedings 457 (1997) 303-308.
6. K. Jia, T.E. Fischer, and B. Gallois, Nanostructured Materials 10[5] (1998) 875-891.
7. H. Moriguchi, K. Tsuduki, and A. Ikegaya, Powder Metallurgy 43[1] (2000) 17-19.
8. M. Omori, Materials Science and Engineering A A287 (2000) 183-188.
9. M. Tokita, Materials Science Forum 308-311 (1999) 83-88.
10. K.R. Anderson, J.R. Groza, M. Fendorf, and C.J. Echer, Materials Science and Engineering A A270 (1999) 278-282.
11. OM Group, Inc., http://www.omgi.com/products/powders/tungsten.html, (2000).
12. L.E. McCandlish, B.H. Kear, and B.K. Kim, Materials Science and Technology 6[10] (1990) 953-957.
13. B.H. Kear, and L.E. McCandlish, Journal of Advanced Materials 10 (1993) 11-19.
14. P. Seegopaul, and L.E. McCandlish, Advanced Powder Metallurgy 3 (1995) 13/3-13/15.
15. E.E. Underwood, “Quantitative Stereology” (Addison-Wesley, 1970).
16. C.B. Ponton, and R.D. Rawlings, Materials Science and Technology 5[9] (1989) 865-872.
17. C.B. Ponton, and R.D. Rawlings, Materials Science and Technology 5[10] (1989) 961-976.
18. D.K. Shetty, I.G. Wright, P.N. Mincer, and A.H. Clauer, Journal of Materials Science 20 (1985) 1873-1882.
19. C.B. Ponton, and R.D. Rawlings, British Ceramic Transactions 88 (1989) 83-90.
20. H.E. Exner, Transactions of the Metallurgical Society of AIME 245[4] (1969) 677-683.
21. J. Dusja, L. Parilak, and M. Slesar, Ceramic International 13[3] (1987) 133.